Supplemental Material

Integrated Optics Waveguides and Mesoporous Oxides for the Monitoring of Volatile Organic Compound Traces in the Mid-Infrared

Felix Frank[1], Bettina Baumgartner[1,2], Mattias Verstuyft[3], Nuria Teigell Beneitez[3], Jeroen Missinne[4], Dries Van Thourhout[3], Gunther Roelkens[3], and Bernhard Lendl[1]*

1 Research Division of Environmental Analytics, Process Analytics and Sensors, Institute of Chemical Technologies and Analytics, TU Wien, Getreidemarkt 9, 1060 Vienna, Austria

2 Van't Hoff Institute for Molecular Sciences, University of Amsterdam, Science Park 904, 1098 XH Amsterdam, The Netherlands

[3] Photonics Research Group, Ghent University-imec, Technologiepark-Zwijnaarde 126, 9052 Gent, Belgium

[4] Center for Microsystems Technology, Ghent University-imec, Technologiepark-Zwijnaarde 126, 9052 Gent, Belgium

***Corresponding author email:** bernhard.lendl@tuwien.ac.at

Synthesis and Characterization of Functionalized Silica Sensing Layers

The sensing layers were prepared by spin-coating three films of mesoporous silica on top of each other using an evaporation-induced self-assembly process (see Experimental Section for procedure). The successful formation of the mesoporous structure of the three films was confirmed by small angle X-ray diffraction (Figure S1). For this, an X'Pert Pro diffractometer equipped with an X'Celerator detector and the Data Collector software (all from PANalytical, Netherlands) were used. The measurements were conducted in Bragg-Brentano geometry using 0.04 rad Soller slits and a divergence slit of 1/4° as well as anti-scatter slits of 1° and 5.0 mm in the incident and diffracted beam path, respectively. The Cu anode was operating at 45 kV and 40 mA. The diffractograms were recorded between 1° and 5° 2θ with a step size of 0.01° and an integration time of 60 s/step in continuous scan mode.

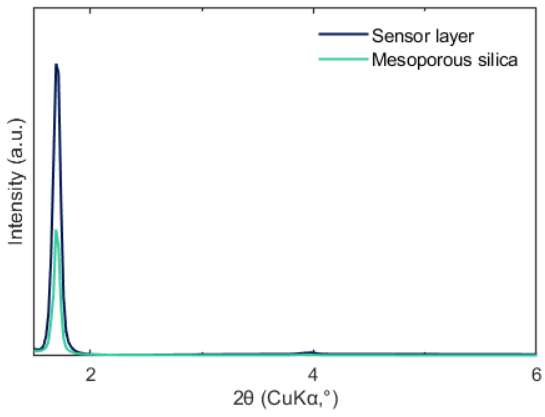

Figure S1. Diffractograms of the mesoporous coating applied to the sensor (blue) and a single mesoporous silica film (green).

As seen in Figure S1, the positions of the peaks do not change with the application of multiple layers, while their intensity increases, hinting on the successful application of the sensing layer. The layer thickness was determined by scanning electron microscopy and profilometry. In Figure S2, a scanning electron microscope cross-section image (10,000x) of a coated waveguide is shown. The cross-section was prepared with a focused ion beam. In this, a layer thickness of 1.71 µm and an etching depth of 900 nm can be determined, which is in line with the values determined by profilometry (1.80±0.05 µm).

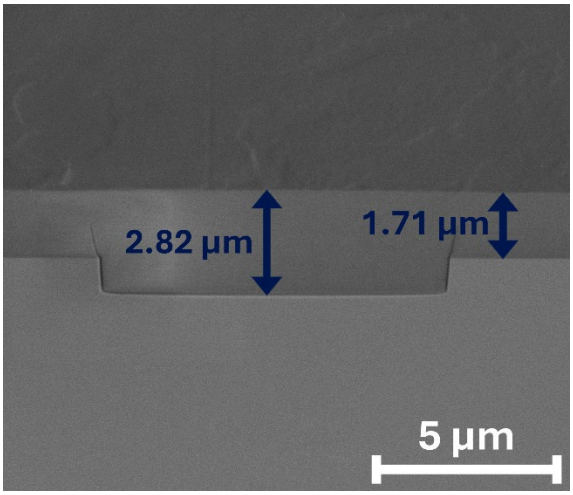

Figure S2. Scanning electron microscopy images of a cross-section of a coated waveguide with an etching depth of 900 nm, recorded with a magnification of 10,000x.

Sensor Calibration

To determine the VOC concentrations of the diluted gas samples, the outlet of the gas mixer was connected to a 4 cm gas transmission cell mounted in a Vertex 70V FT-IR spectrometer (Bruker, Germany) equipped with a liquid nitrogen cooled mercury cadmium telluride (MCT) detector. For the calibration of the sensor, different mixtures of the three VOCs were applied. For the pure samples, the sample gas reservoir was evacuated and flushed numerous times. However, as the VOCs were injected in their liquid state, there was still a high probability of contaminations. In Figure S3-Figure S5 below, examples for such pure QCL-IR spectra with slight contaminations are shown. Further, the enrichment profiles for the experiments are displayed.

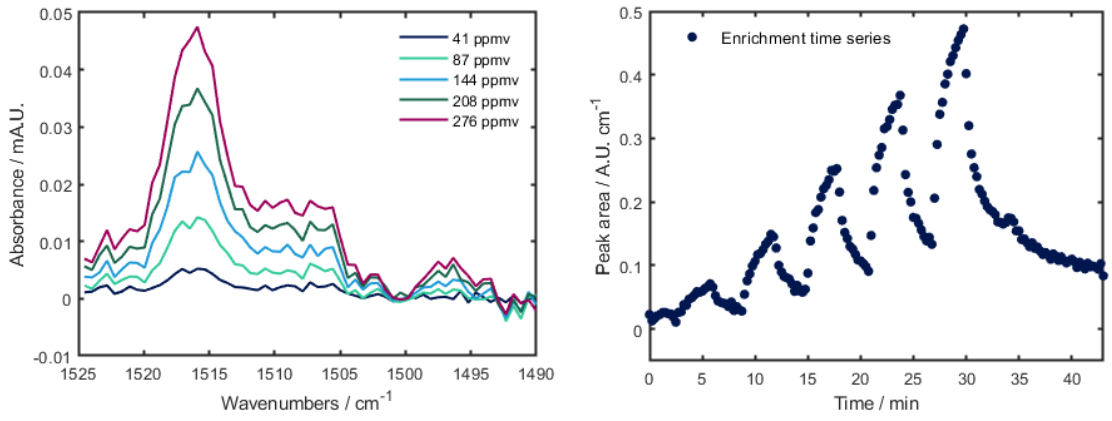

Figure S3. QCL-IR waveguide spectra for different concentrations of p-Xylene with slight 1,2,4-Trimethylbenzene and Toluene impurities (left) and enrichment profiles for the duration of the calibration experiments (right).

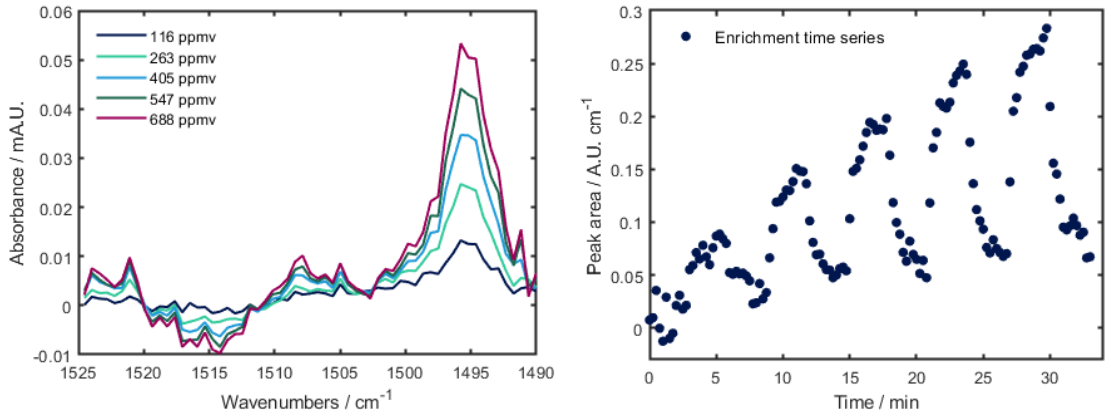

Figure S4. QCL-IR waveguide spectra for different concentrations of Toluene (left) and enrichment profiles for the duration of the calibration experiments (right).

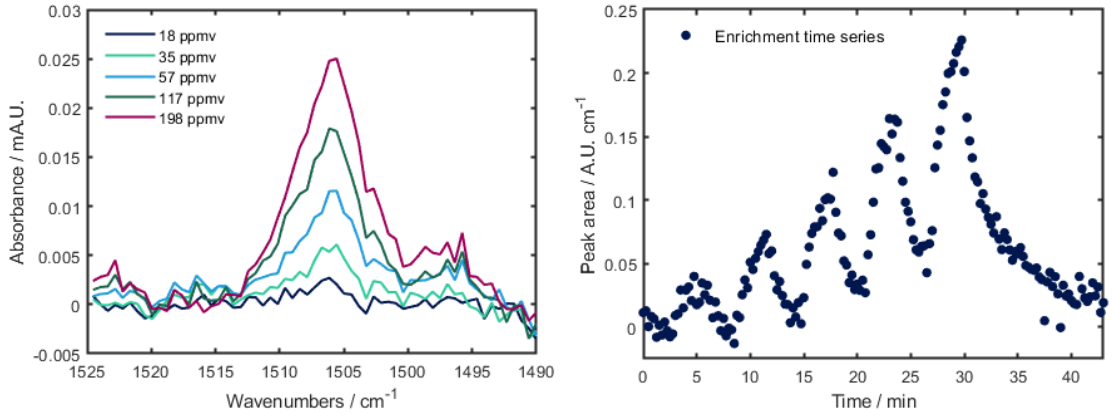

Figure S5. QCL-IR waveguide spectra for different concentrations of 1,2,4-Trimethylbenzene with slight Toluene impurities (left) and enrichment profiles for the duration of the calibration experiments (right).

In Table S1, the fit parameters for each respective VOC are given. $K_{F'}$ and n_F are the Freundlich model constants as shown in (1), while the values in brackets for the LODs refer to the 95% confidence boundaries for the respective fits.

Table S1. Fit parameters and limit of detection (LOD) for the sensor calibration.

	p-Xylene	Toluene	1,2,4-Tri-methylbenzene
k_f / cm^{-1} A.U.	0.00663	0.00073	0.00169
n_F / a.u.	1.428	1.182	1.496
LOD / ppmv	0.14 (0.05;0.46)	2.14 (1.28;5.85)	0.88 (0.33;3.34)

Stability to Water Vapor Traces

The broad spectral region of water vapor bands traces makes it very challenging for trace analysis of VOCs in the presence of even small traces of water vapor. In Figure S6, this is shown at the example of a gas mixture of 144 ppm p-xylene with water vapor traces of 350 ppm present when measured in transmission on an FT-IR spectrometer. As some of the water vapor absorption bands are located within the spectral region of interest

for VOC sensing, they interfere with the quantification of the actual analytes. On the other hand, looking at the spectrum measured with the sensor, the advantages of the sensing platform can be seen very clearly, with no water vapor traces interfering with the measurement, and also the enrichment of the analyte in the probed volume of the waveguides, with the signal being much higher than for the transmission cell, considering an even lower interaction path length of the waveguide.

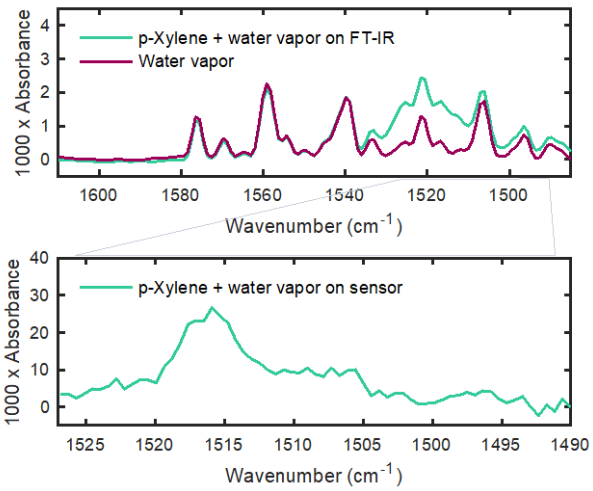

Figure S6. FT-IR transmission gas spectrum of gas mixture of 144 ppm toluene with 350 ppm water vapor traces and 350 ppm water vapor reference spectrum (top), QCL-IR spectrum of gas mixture of 144 ppm toluene with 350 ppm water vapor traces.

Evaluation of Different Chemometric Models

For the determination of the VOC concentrations, NNLS was not feasible due to the lack of pure spectra and it not being possible to fit the peaks with simple Lorentzian functions. In Figure S7, the deconvoluted FT-IR transmission spectra for the VOC mixtures are shown. In Figure S8, the MCR-ALS loadings are shown, which can be used to calculate the respective peak areas and concentrations via comparison with the PNNL database shown in Figure S9. The concentrations for all tested gas mixtures (each spectrum on the x-axis in Figure S8 and Figure S9 equates to one gas mixture) are shown in Table S 2, with the concentrations used for sensor calibration marked in bold.

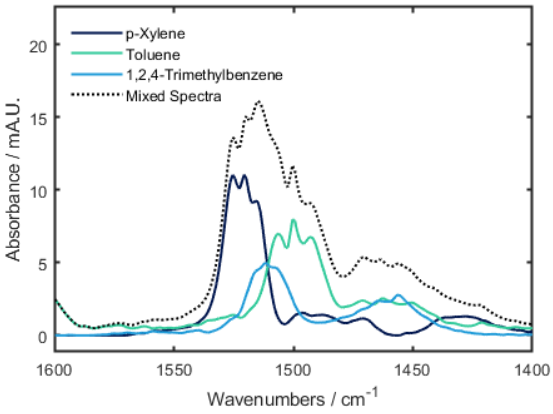

Figure S7. Deconvoluted spectra for the transmission gas spectra.

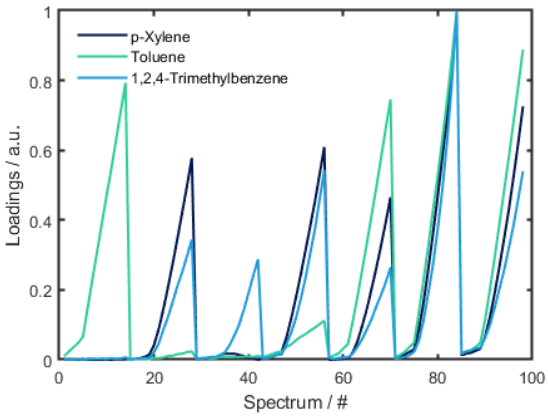

Figure S8. MCR-ALS loadings for the transmission gas spectra.

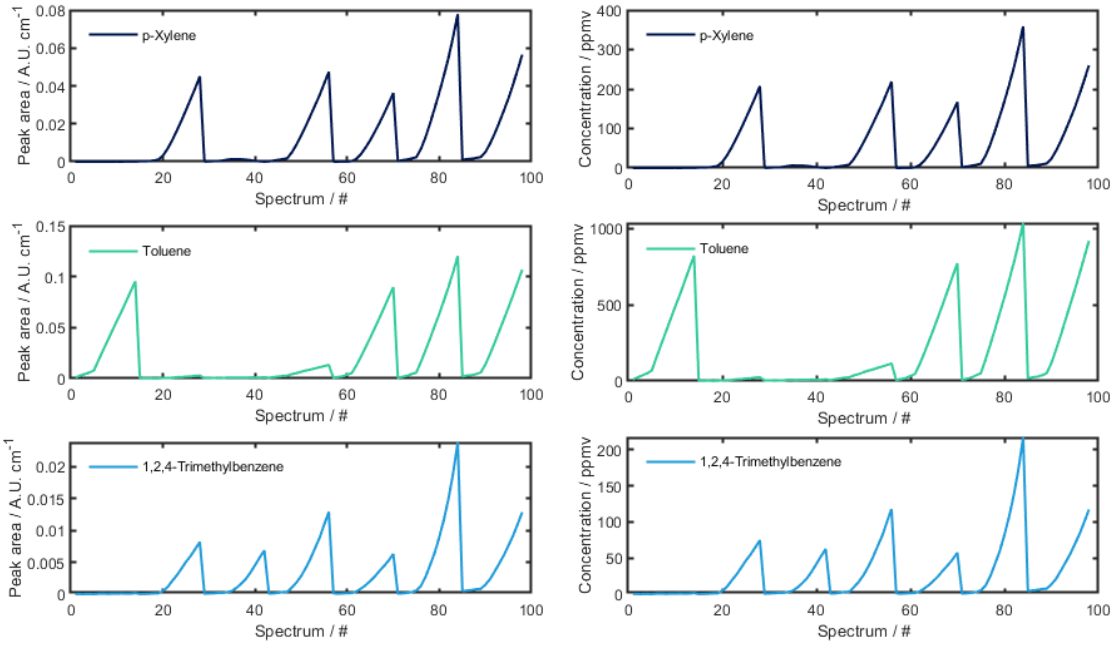

Figure S9. Deconvoluted peak areas (left) and concentrations for the respective gas mixtures (right).

Table S2. Concentrations as calculated for the respective gas mixtures, concentrations used for sensor calibration marked in bold, concentrations not used for sensor calibration marked in grey.

	% mix	2	4	6	8	10	20	30	40	50	60	70	80	90	100
Mixture 1	c_{Xyl} / ppmv	0	0	0	0	**0**	**0**	**0**	**0**	**0**	1	0	1	1	1
	c_{Tol} / ppmv	1 8	4 0	6 3	8 5	**11 6**	**26 3**	**40 5**	**54 7**	**68 8**	82 9	964	110 8	125 5	139 6
	c_{Tmb} / ppmv	0	0	0	1	**0**	**2**	**2**	**2**	**2**	2	3	3	3	6
Mixture 2	c_{Xyl} / ppmv	1	2	4	4	8	14	**17**	**17**	**17**	14	**10**	6	**3**	0
	c_{Tol} / ppmv	6	7	9	7	8	13	**14**	**12**	**14**	14	**15**	16	**14**	19
	c_{Tmb} / ppmv	2	4	5	7	7	11	**18**	**35**	**57**	82	**117**	157	**198**	236
Mixture 3	c_{Xyl} / ppmv	3	3	4	8	14	**41**	**87**	**14 4**	**20 8**	**27 6**	348	421	496	574
	c_{Tol} / ppmv	3	4	5	2	3	**9**	**8**	**12**	**19**	**21**	28	30	39	41
	c_{Tmb} / ppmv	0	1	2	4	4	**17**	**38**	**71**	**10 1**	**13 7**	175	207	244	282
Mixture 4	c_{Xyl} / ppmv	2	7	**1 2**	1 7	**23**	**64**	**11 6**	**17 6**	24 0	30 8	378	448	527	605
	c_{Tol} / ppmv	1 1	2 0	**2 9**	3 7	**40**	**63**	**77**	**97**	11 5	12 8	146	161	179	197
	c_{Tmb} / ppmv	3	4	**7**	1 1	**12**	**36**	**64**	**98**	14 1	19 1	248	305	376	445
Mixture 5	c_{Xyl} / ppmv	0	0	**1**	1	**4**	**20**	**52**	**96**	14 5	20 2	261	325	391	462
	c_{Tol} / ppmv	1 1	2 2	**3 1**	5 6	**79**	**19 0**	**31 6**	**45 1**	58 6	72 8	869	101 7	116 7	131 2
	c_{Tmb} / ppmv	4	2	**4**	5	**6**	**14**	**30**	**48**	71	96	126	152	182	217
Mixture 6	c_{Xyl} / ppmv	5	1 0	**1 5**	**2 2**	**30**	**86**	**16 4**	26 0	36 1	46 7	580	702	841	994
	c_{Tol} / ppmv	1 2	2 5	**3 9**	**6 5**	**86**	**23 9**	**40 5**	57 6	75 6	93 1	112 1	131 6	152 9	176 0
	c_{Tmb} / ppmv	3	4	**7**	**1 0**	**19**	**45**	**93**	15 7	22 4	30 9	404	518	655	821

		1	1	2	2			12	18	26	34				
	c_{Xyl} / ppmv	3	7	0	5	31	65	1	8	3	4	426	520	618	721
		3	4	4	6		20	35	51	68	85	102	119	138	156
Mixture 7	c_{Tol} / ppmv	0	2	8	4	87	1	2	2	0	0	0	7	0	3
	c_{Tmb} /	1	1	2	2				12	16	21				
	ppmv	6	9	2	6	28	51	81	2	6	0	262	316	379	444

Comparing the two chemometric algorithms for the sensor calibration, overfitting for the MCR-ALS algorithm was already discussed in the main paper. In Figure S10, the results of the deconvolution with NNLS and MCR-ALS are compared, showing lower residual values for the MCR-ALS model as well as the deviation from the theoretical Lorentzian peak shapes. Looking at the distribution of residuals of the predictive fit for each of the VOCs for the two algorithms in Figure S11 (for the NNLS model) and Figure S12 (for the MCR-ALS model), NNLS delivers better resemblance to a gaussian shape for p-Xylene, whereas it is quite similar for the other two VOCs.

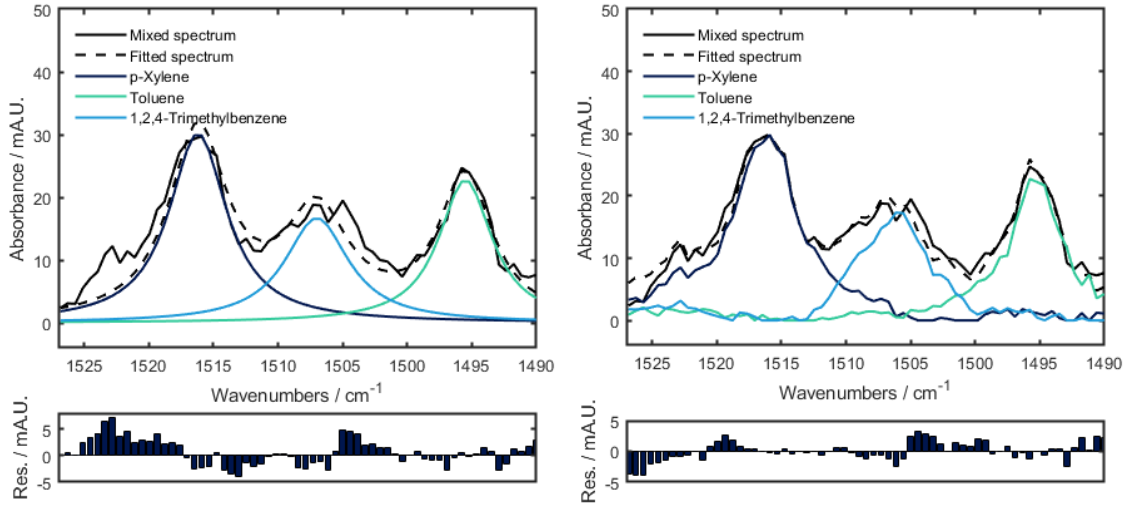

Figure S10. Comparison of the VOC spectra of the mixture acquired with the QCL based VOC sensor fitted by NNLS (left), and MCR-ALS (right). Sum spectrum of the three fits in dashed line. Residual plot of the fit (bottom).

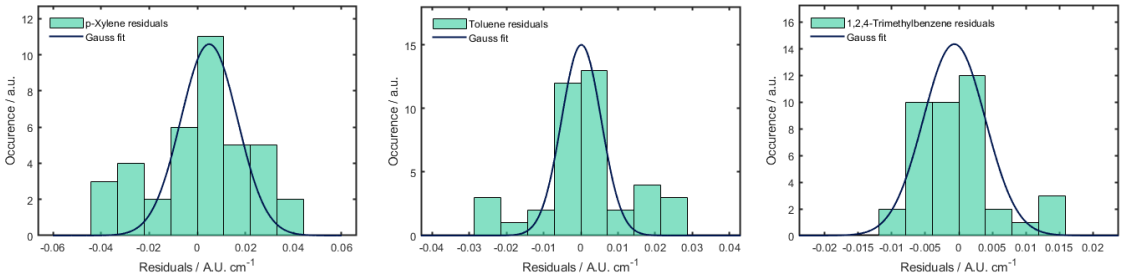

Figure S11. Residuals for the NNLS model.

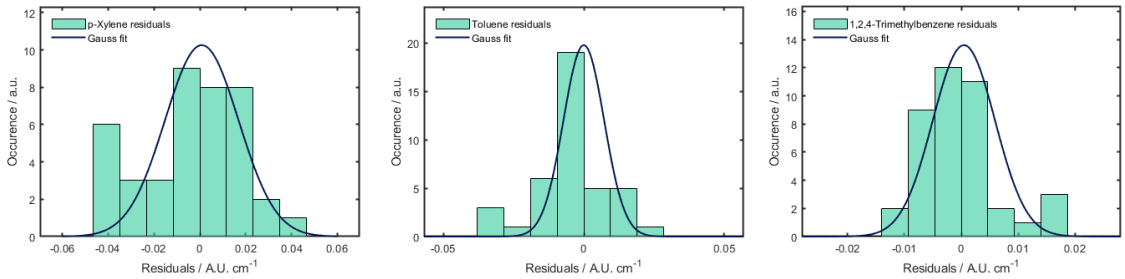

Figure S12. Residuals for the MCR-ALS model.

The residuals were fitted with a simple gaussian function (Table S 3) and their empirical cumulative distribution function compared to the simulated cumulative distribution function (Figure S13 for the NNLS model, Figure S14 for the MCR-ALS model).

Table S3. Fit parameters for gaussian fitting of residuals, all units in A.U.cm^{-1}.

	NNLS			MCR-ALS		
	p-Xylene	Toluene	1,2,4-Trimethylbenzene	p-Xylene	Toluene	1,2,4-Trimethylbenzene
A	10.5910	15.0011	14.3437	10.2602	16.3195	13.6033
mu	0.0050	0.0002	-0.0007	0.0009	-0.0004	0.0005
sigma	0.0118	0.0054	0.0046	0.0161	0.0048	0.0055

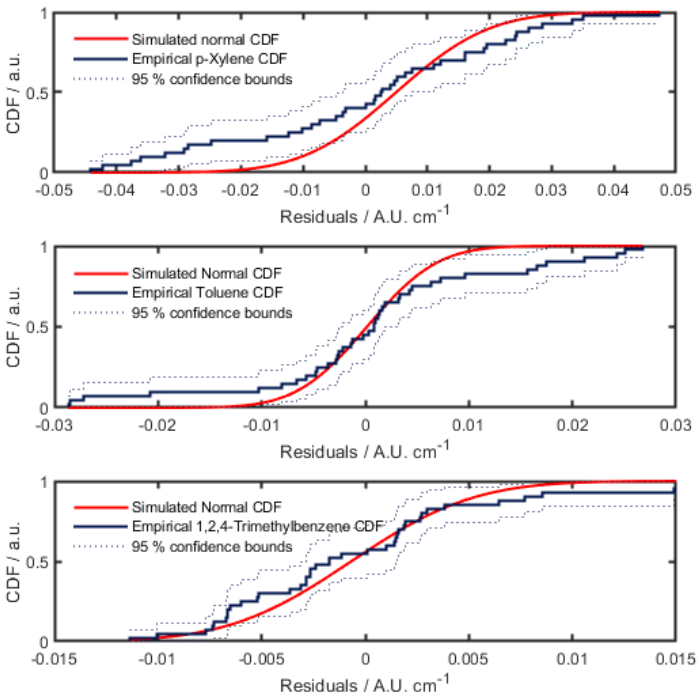

Figure S13. Comparison of the empirical and simulated cumulative distribution function for the NNLS model.

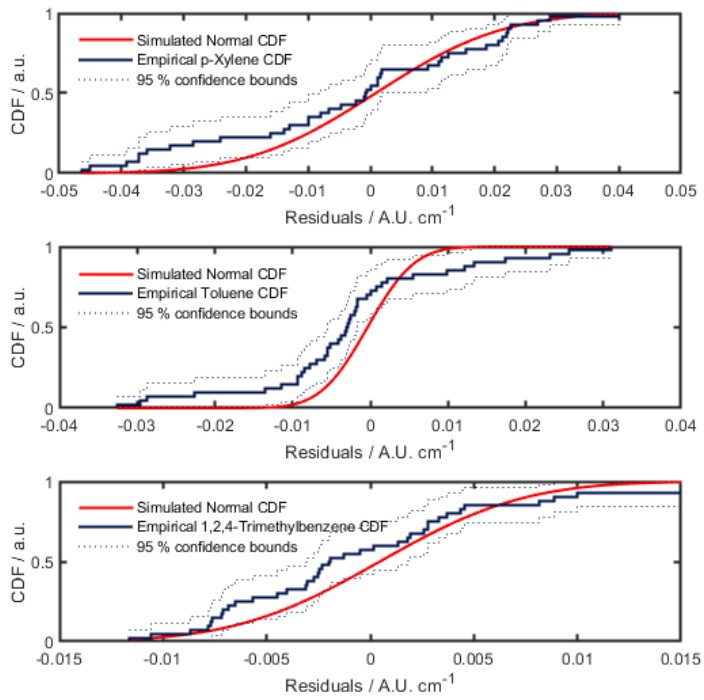

Figure S14. Comparison of the empirical and simulated cumulative distribution function for the MCR-ALS model.

To check the residuals for normal distribution, a one-sample Kolmogorov–Smirnov was performed for each VOC and algorithm, respectively. The α-Value was set to 5% for each respective test, and the results for the statistical tests are shown in Table S 4.

Table S4. Statistical parameters for the normal distribution test of the residuals.

	NNLS			MCR-ALS		
	p-Xylene	Toluene	1,2,4-Trimethylbenzene	p-Xylene	Toluene	1,2,4-Trimethylbenzene
p-Value	0.0856	0.1613	0.4654	0.1978	0.0030	0.0861
Accepted	✓	✓	✓	✓	✗	✓